Characteristics of Gamma-ray Air Showers around 10^{20}eV

N. Inoue, K. Shinozaki and H.P. Vankov[1]

Department of Physics, Saitama University, Saitama 338-8570, Japan
[1]*Institute for Nuclear Research and Nuclear Energy, Sofia, Bulgaria*

(Received October 19, 2001)

Longitudinal developments of gamma-rays with energies less than $10^{19.5}$eV show slower profiles and their shower maxima are deeper than ones expected from proton initiated air showers. At higher energy region, shower developments initiated by gamma-rays become to be much slower in average with larger fluctuations because the LPM effect gives important contribution on such longitudinal development. Shower developments become to be slower in average with larger fluctuations. Simultaneously, primary gamma-ray with an energy greater than several times 10^{19}eV has a probability to make interaction with the geomagnetic field and then it produces a geomagnetic cascading before entering to the atmosphere. Interaction probability and multiplicity of secondary particles in geomagnetic cascading are strongly depend on primary gamma-ray energy and a strength of geomagnetic field which actually related to an arrival direction. In this case, shower development is formed by a superposition of sub-showers with $\sim 1\%$ of primary energy. Shower developments of gamma-ray primaries are affected by both effects and show characteristic profiles depend on primary energy and arrival direction.

KEYWORDS: ultra-high-energy, cosmic-ray, gamma-ray, air shower, geomagnetic field

§1. Introduction

The primary composition of UHE cosmic rays is one of unsolved problems in high energy particle astrophysics. Various models have been proposed as UHE cosmic ray origin: active astrophysical object (Rachen, 1993,[1)]), decay products of much higher energy particles such as super-heavy relic particles (Berezinsky, 1997 [2)]) or topological defects (Bhattacharjee, 1992 [3)]), and they have predicted the presence of gamma-ray primaries in the highest energy region, whose flux depends much on the models of their production or propagation in the intergalactic space.

In case of gamma-ray primaries, an influence of the Landau-Pomeranchuk-Migdal (LPM) effect (Landau, 1953 [4)] and Migdal,1956 [5)]) on shower development has been studied and applied for simulation works by many authors. In general, this effect is an important mechanism to bremmsstrahlung and pair creation processes at extremely high energies to make characterize the gamma-ray shower development.

Another effect is a cascading in the geomagnetic field. A history of these calculations is long enough too and it started with the work by McBreen and Lambert,1981 .[6)] Recent calculations (Stanev,1997 [7)]) refined the previous ones revealing some practically important features in the cascading process.

§2. Simulation of UHE Gamma-ray Shower

To study on features of air shower developments initiated by UHE gamma-rays and hadrons (proton or iron) the AIRES simulation code(Ver.2.2.1;Sciutto, 1999 [8)]) with QGSJET hadronic interaction model has been used in this work. In addition we made out our own code for electromagnetic cascading in the geomagnetic field. To simulate showers initiated by UHE gamma-rays, first we modeled cascading in the geomagnetic field starting with a single UHE gamma-ray far away from the Earth's surface down to the top of the atmosphere and connected to shower generated by AIRES.

The essentially non-zero probabilities for magnetic bremsstrahlung and pair production are required in cases of strong geomagnetic field or high energy primary gamma-ray (Erber,1966 [9)]). The relevant parameter determining the criteria is:

$$\chi = \frac{\varepsilon}{mc^2}\frac{H}{H_{cr}}$$

where ε is the particle energy, H is the magnetic field strength (the component normal to the particle trajectory), m is the electron mass and $H_{cr} = 4.41 \times 10^{13}$ G.

The total probabilities (cross sections) for radiation and pair production for a given value of the magnetic field strength depend only on χ are shown on fig.1. Magnetic pair production has significant probability for $\chi \geq 0.1$ but for effective shower development one needs even higher values of χ ($\chi \geq 1$) because the radiated photon spectrum becomes harder with increasing χ. The maximal photon energy ($\sim$ 6x10^{19}eV) comes from the condition $\chi \sim 1$.

We used the differential probabilities (per unit length) for magnetic bremsstrahlung and magnetic pair production given by the expressions (Bayer,1973 [10)]):

$$\pi(\varepsilon,\omega)\,d\omega = \frac{\alpha m^2}{\pi\sqrt{3}}\frac{d\omega}{\varepsilon^2}\times \left[\left(\frac{\varepsilon-\omega}{\varepsilon}+\frac{\varepsilon}{\varepsilon-\omega}\right)K_{\frac{2}{3}}\left(\frac{2u}{3\chi}\right)-\int_{\frac{2u}{3\chi}}^{\infty}K_{\frac{1}{3}}(y)\,dy\right] \quad (2.1)$$

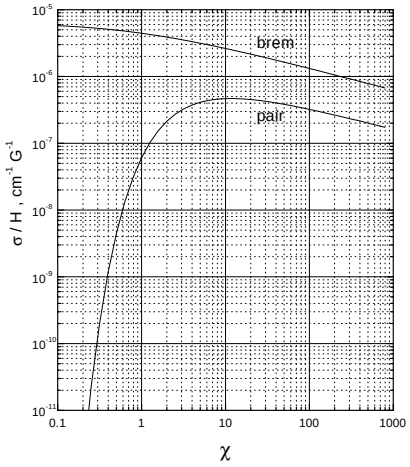

Fig. 1. The total probabilities (cross sections) for magnetic bremsstrahlung and pair production as a function of χ.

$$\gamma(\omega,\varepsilon)\,d\varepsilon = \frac{\alpha m^2}{\pi\sqrt{3}}\frac{d\varepsilon}{\omega^2}\times$$
$$\left[\left(\frac{\omega-\varepsilon}{\varepsilon}+\frac{\varepsilon}{\omega-\varepsilon}\right)K_{\frac{2}{3}}\left(\frac{2u_1}{3\chi}\right)+\int_{\frac{2u_1}{3\chi}}^{\infty}K_{\frac{1}{3}}(y)\,dy\right] \quad (2.2)$$

where ε and ω are the electron and photon energies and $u=\frac{\omega}{\varepsilon-\omega}$, $u_1=\frac{\omega^2}{\varepsilon(\omega-\varepsilon)}$. Here $\hbar=c=1$.

$K_\nu(z)=\int_0^\infty e^{-zch(t)}\mathrm{ch}(\nu t)\,dt$ is a modified Bessel function known as MacDonald's function.

While for $\chi \gg 1$ (strong field) the electromagnetic cascade develops similarly to the cascade in matter, in the region of $\chi \leq 1$ (geomagnetic field) the gamma-ray interaction length increases sharply with decrease of gamma-ray energy. Electrons continue to radiate and the shower becomes a bunch of secondary gamma-rays carrying $\geq 94-95\%$ of the primary energy.

In our simulation we used the International Geomagnetic Reference Field (IGRF) and World Magnetic Model (WMM) which provides a good approximation of the geomagnetic field up to 600 km from the ground and its extrapolation above this altitude. In this paper the properties of UHE gamma-ray showers are examined for the location of Utah, USA(133.0^{o}W, 39.5^{o}N and 1500m a.s.l.) .

We simulated the electromagnetic cascading by injecting UHE gamma-ray at a distance of 3 Earth's radii from the surface of the Earth. Primary gamma-ray and secondary particles were propagated with pair production and radiation taken into account on each step(a step-size of 1km). Only particles above the threshold energy of 10^{15}eV were followed in the simulation until they reach the top of the atmosphere.

Interaction probabilities of incident gamma-rays with the geomagnetic field have been estimated for different zenith and azimuthal angles of the arrival direction. Fig.2 shows probability maps for gamma-ray conversion for 3 different primary energies in horizontal coordinates. The region with a smaller probability is centered at 29^o in a zenith angle and a direction of 14^o west from the south which corresponds to the inverse direction of geomagnetic field. The size of this "window" shrinks quickly with an increase of primary energy, and most primary gamma-rays with energies greater than 10^{20}eV build the geomagnetic cascade before the top of atmosphere. Fig.3 shows energy weighted spectra of secondary particles in geomagnetic cascading at the top of atmosphere for primary gamma-ray energies of $10^{19.5}$, $10^{20.0}$, $10^{20.5}$ and $10^{21.0}$eV drawn in each frame. Zenith angles are sampled as 54.0° and 61.6° and azimuthal angles are assumed as north and south. Features of energy weighted spectra strongly depend on the arrival directions and primary energy. Primary gamma-rays without interaction to geomagnetic field can be found at the right end of energy weighted spectra in specific cases.

Successive shower developments in the atmosphere are constructed as a superposition of sub-showers initiated by secondary particles represented in energy spectra.

First library of sub-showers initiated by gamma-rays with energy between 10^{16}eV and 10^{21}eV was prepared by AIRES. Primary energies of gamma-rays are assigned with a log step of 0.1 over an energy range and 500 showers have been simulated for each entry. The number of electrons and all charged particles for each shower was recorded at every 5 g/cm^2 step in vertical depth. Construction of UHE gamma-ray initiated shower in the atmosphere has been done by the following procedure. i-th secondary particle with energy $E_i^{(\mathrm{gm})}$ at the top of atmosphere is replaced by the sub-shower with the nearest energy $E_i^{(\mathrm{atm})}$ selected randomly from the library. The secondary electron is replaced by a gamma-ray with same energy. By summing up the sub-showers ($i=1,\ldots,N_\gamma^{(\mathrm{gm})}$) with a weight $w_i=E_i^{(\mathrm{gm})}/E_i^{(\mathrm{atm})}$, atmospheric air shower initiated by a single gamma-ray with energy $E_0^{(\gamma)}$ is constructed as a superposition of sub-showers with total energy of $\sum^{N_\gamma} w_i E_i^{(\mathrm{atom})}$.

§3. Results and Discussion

Maps of average X_{max}(an atmospheric depth at the shower maximum:$\langle X_{max}\rangle$) for 3 different primary energies of gamma-rays in horizontal coordinates are shown in fig.4. $\langle X_{max}\rangle$ is related to an integration of magnetic field component perpendicular to a trajectory of cascading even if primary energy is fixed. Relation between $\langle X_{max}\rangle$ of gamma-ray shower and primary energy is shown in fig.5 together with ones of proton and iron showers. $\langle X_{max}\rangle$s of gamma-ray primaries have been calculated for zenith angles of 54.0^o and 61.6^o(a broken and a solid line,respectively) and cases of south/north arrival directions are drawn in the figure. Ones of pro-

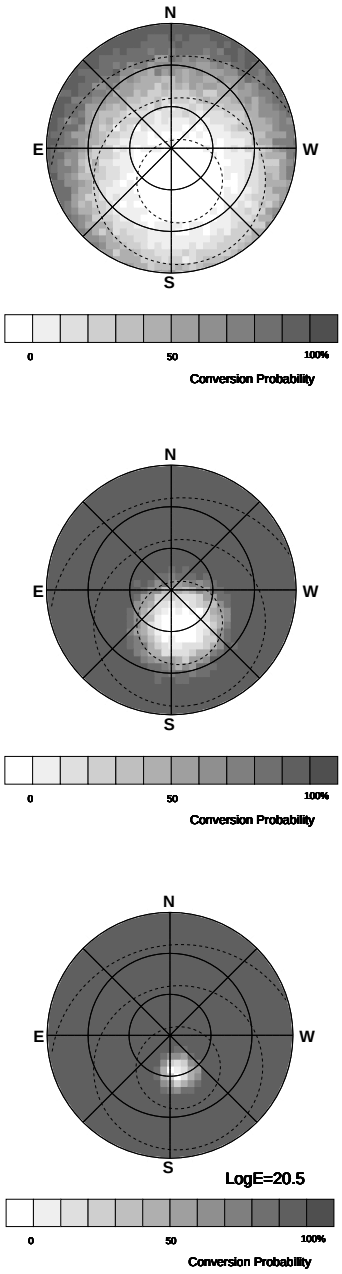

Fig. 2. Maps of gamma-ray conversion probability for primary gamma-ray energies of $10^{19.5}$eV, $10^{20.0}$eV and $10^{20.5}$eV in horizontal coordinates. Inner circles show zenith angles of 30° and 60° and horizon. Dashed lines correspond to the angular distances of 30°, 60° and 90 ° to the inverse direction of geomagentic field at Utah.

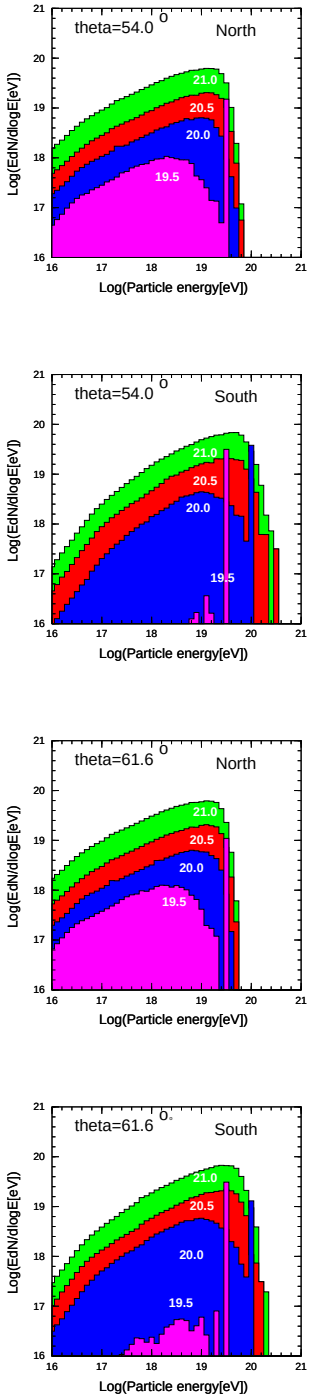

Fig. 3. Energy weighted spectra of secondary particles at the top of atmosphere for primary gamma-ray energies of $10^{19.5}$eV, $10^{20.0}$eV, $10^{20.5}$eV and $10^{21.0}$eV with 2 different zenith angles(54.0° and 61.6°). Azimuthal angles of primary gamma-rays are assumed as north and south.

ton and iron primaries are also plotted with a solid and a dotted line. $\langle X_{max}\rangle$s of proton and iron showers are increasing with constant elongation rates of $54.2gcm^{-2}$ and $56.0gcm^{-2}$ over an energy range up to 10^{20}eV, and also ones of gamma-ray showers indicate a larger value with invariable elongation rate up to $\sim 2\times10^{19}$eV. However, if the geomagnetic cascading process is not applied in the calculation an elongation rate in higher energy region becomes larger with increasing gamma-ray energy as shown by open circles. The geomagnetic cascading actually starts its contribution to shower development from several times 10^{19}eV depending on the arrival direction of gamma-ray, and then $\langle X_{max}\rangle$s decrease and reach at the minima because shower developments in atmosphere are almost equivalent to those of gamma-ray showers with a dominant energy of secondary component at the top of atmosphere. $\langle X_{max}\rangle$s increase again after the minima because an average energy of secondary par-

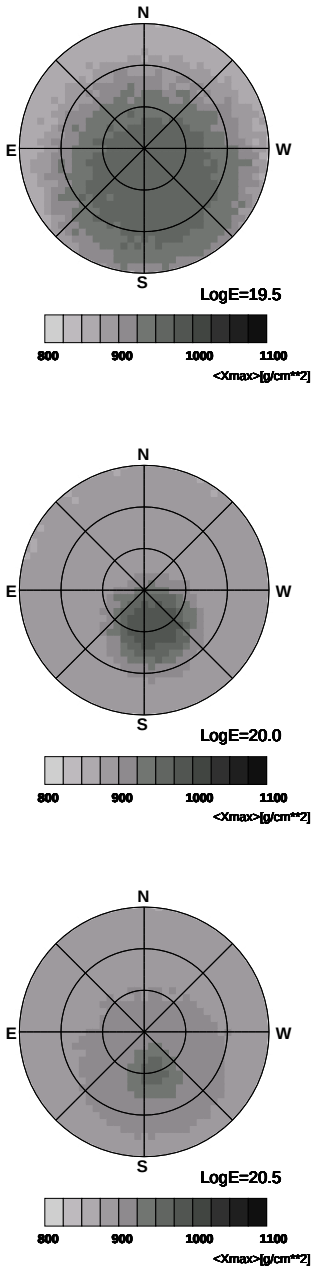

Fig. 4. Maps of $< X_{max} >$ for primary gamma-ray energies of $10^{19.5}$eV, $10^{20.0}$eV and $10^{20.5}$eV in horizontal coordinates.

ticle becomes higher with increasing primary gamma-ray energy.

Fluctuations of X_{max} as a function of primary energy are shown for proton, iron and gamma-ray primaries in fig.6. standard deviation(σ) of proton and iron primaries are plotted by a broken and a dotted line, respectively. Zenith angles of 54.0^o and 61.6^o are assumed for gamma-ray primaries shown in top and bottom frames, respectively. Closed and open circles show the standard deviations for cases of azimuthal directions of south and north in both frames. Though proton and iron showers have almost constant σ values of $67gcm^{-2}$ and $26gcm^{-2}$ over an energy range above 10^{18}eV, ones of gamma-rays have characteristic features depend on their primary energies.

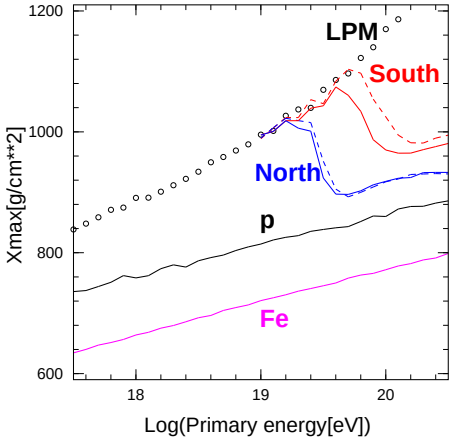

Fig. 5. Average X_{max} for showers initiated by protons, irons and gamma-rays as a function of primary energy. Proton and iron showers were simulated with AIRES-QGSJET. X_{max} of gamma-ray showers from south and north with zenith angles of 54.0°(broken line) and 61.6°(solid line) are shown.

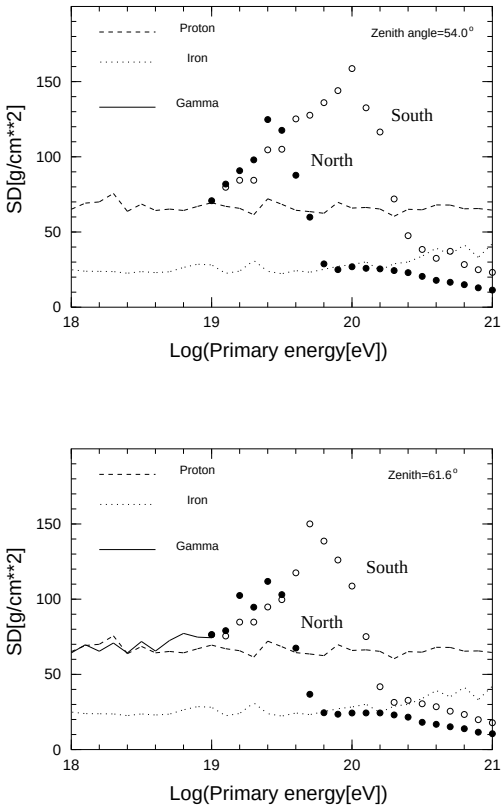

Fig. 6. Fluctuations(standard deviation:σ) of X_{max} as a function of primary energy. Proton, iron and gamma-ray primaries with zenith angles of 54.0^o and 61.6^o are assumed in the calculation. For gamma-ray primary fluctuations are drawn for cases of showers coming from south and north directions.

Dominant contribution in larger fluctuation seen in an energy region between 19^{19}eV and 10^{20}eV is the influence of the mixed shower developments which are characterized by geomagnetic cascading on and off. Fluctuation decreases quickly and reaches at the minimum within a change of primary energy less than $\Delta \log E_o$ of 0.5. Smaller fluctuation can be found in a higher energy region, as a result of shower developments which are constructed by a superposition of sub-showers initiated by secondary geomagnetic cascading particles.

X_{max} distributions for showers initiated by protons and gamma-rays with energies of $10^{20.0}$ and $10^{20.5}$eV and zenith angles of 54.0^o and 61.6^o are shown in fig.7. An ambiguity of experimental determination in X_{max} is assumed and included as $30 gcm^{-2}$ in these distributions. X_{max} distributions of gamma-rays also are not simple features. They are changeable with primary energies and arrival directions because X_{max} of shower developments are affected by energy spectra of secondary particles in geomagnetic cascading. As seen in fig.7, if primary gamma-rays interact with geomagnetic field and build up enough developed geomagnetic cascading seen in cases of showers coming from north with energies greater than 10^{20}eV, a smaller fluctuation of X_{max} is expected, which is narrower than that of proton showers. X_{max} distributions of gamma-rays coming from south have different features for any case of primary energies and arrival directions because they are composed of shower developments with rather weak or no contribution of geomagnetic cascading.

Telescope Array experiment is proposed to study on the origin and nature of UHE cosmic rays with a large statistics of observed events. The estimated annual event rates of cosmic rays are 2000, 350 and 70 for energy regions of 1×10^{19}eV $- 3 \times 10^{19}$eV, 3×10^{19}eV $- 10^{20}$eV and $> 10^{20}$eV, respectively. The detection possibility of characteristic features contributed from gamma-rays as one of assumed primary compositions, depends on total statistics of expected cosmic rays and assumed gamma-ray flux in an overall energy spectrum. As seen in fig.5, $\langle X_{max} \rangle$ of gamma-ray initiated showers is much larger than that expected from proton initiated showers in an energy region less than 10^{19}eV. Furthermore, the elongation rates of gamma-ray showers show significant changes at higher energy region depending on their arrival directions. These properties of $\langle X_{max} \rangle$ in relation to primary energy and arrival direction are possible keys to study the gamma-ray flux in the total cosmic ray flux through the observable of $\langle X_{max} \rangle$ which will be determined with smaller mean errors expected in an energy region between 10^{19} and 10^{20}eV. Also, behaviors of X_{max} fluctuations should be taking into account as one of parameters to characterize the feature as an additional information to $\langle X_{max} \rangle$ as seen in fig.6. A study in an energy region greater than 10^{20}eV may need more elaborate considerations to acquire a definite conclusion because of insufficient statistics and smaller difference in shower profiles between gamma-ray and proton primaries. A study on individual shower profiles which will be measured with the best accuracy by Telescope Array at the highest energy region, will be preferable to discuss in paying an attention to their arrival directions as the first step. Detection efficency of contributed gamma-ray signals as one of primary compositions in expected shower properties mentioned before, has been evaluated with a statistical significance and it is in progress with careful examinations of nuclear interaction models in simulation and experimental uncertainties to determine X_{max} and primary energy for gamma-ray showers.

1) Rachen,J.P. and Biermann,P.L., *1993, Astrophys.,* **272**, 161
2) Berezinsky,V.,Kachelriess,M. and Vilenkin,A. *,1997, Phys. Rev. Lett.*, **79**, 4302
3) Bhattacharjee,P.,Hill,C.T. and Schramm,D.N. *,1992, Phys. Rev. Lett.*, **69**, 567
4) Landau,L.D. and Pomeranchuk,I.J. *,1953, Dokl. Akad. Nauk. SSSR*, **92**, 535
5) Migdal,A.B. *,1956, Phys. Rev.*, **103**, 1811
6) McBreen,B. and Lambert,C.J. *,1981, Phys. Rev. D*, **24**, 2536
7) Stanev,T. and Vankov,H.P. *,1997, Phys. Rev. D*, **55**, 1365
8) Sciutto,S.J. *,1999, GAP99-044*, AUGER technical note
9) Erber,T., *,1966, Rev. Mod. Phys.* **38** 626
10) Bayer,V.H., Katkov,B.M. and Fadin,V.S., *,1973, Radiation of relativistic electrons(Moscow:Atomizdat)*

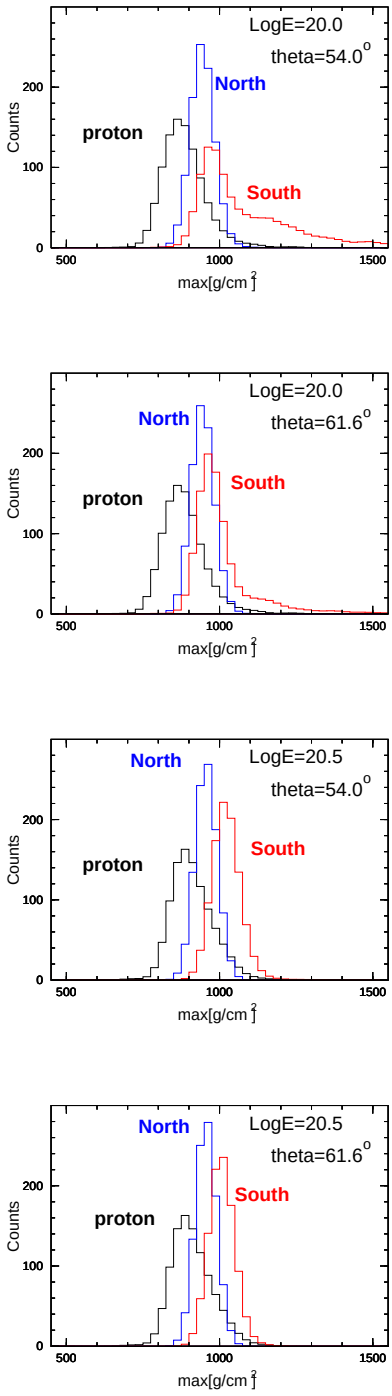

Fig. 7. X_{max} distributions for proton and gamma-ray showers with energies of 10^{20}eV and $10^{20.5}$eV. Zenith angles of 54.0^o and 61.6^o are assumed and ones of gamma-ray showers are plotted with arrival directions of south and north in each figure. An ambiguity of experimental determination in X_{max} is included as $30gcm^{-2}$ in these distributions.